Final report

Hydrogen embrittlement resistance of 316L stainless steel with different chemical compositions

Submitted by

Junhe Lian

Advanced Manufacturing and Materials

Department of Mechanical Engineering

School of Engineering

Aalto University

1. Objectives

Nowadays, hydrogen embrittlement (HE) has caused severe material failure and economic loss every year. Due to the widespread application of 316L stainless steel, the HE-caused failures of 316L stainless steel have attracted much attention from researchers. The aim of this research is to try to improve the HE resistance of 316L stainless steel by altering the chemical composition.

The results obtained in this study provide a better understanding of how chemical composition affects the HE resistance of 316L stainless steels and can be useful in the future design of materials. Since a loss of ductility has been observed, it is essential to carefully consider the effect of hydrogen in the selection of materials for hydrogen storage and transport applications.

2. Materials and experiments

2.1 Materialscomposition of 316L stainless steel 4420 and 4404. The main difference between the two materials is their respective weight percentage of Mn, Cr, and Mo elements.

Table 1 shows the chemical composition of 316L stainless steel 4420 and 4404. The main difference between the two materials is their respective weight percentage of Mn, Cr, and Mo elements.

Table 1 Chemical composition of 316L stainless steel 4420 and 4404 (wt. %)

Type	C	Si	Mn	Al	Cr	Mo	Ni	Fe
4420	0,01	0,45	1,701	0,005	20,15	0,567	8,35	Bal.
4404	0,012	0,612	0,907	0,007	17,18	1,994	9,43	Bal.

The metal sheets (*Outokumpu company*) supplied for this study are manufactured in cold-rolled form. The raw material is first passed through a series of cleaning and pre-treatment steps such as pickling, descaling, or applying a lubricant to the metal surface to prevent damage and reduce friction during rolling. The metal is then fed through a set of rollers that apply pressure to the metal, reducing its thickness and increasing its strength and hardness.

2.2 Hydrogen charging

To investigate the effect of hydrogen diffusion on mechanical properties, the hydrogen charging (HC) process is essential. In this project, the solution used is an acidic aqueous solution with a concentration of 1N H_2SO_4. To this solution, 20 mg/L thiourea (CH_4N_2S) is added as “hydrogen poison”, and acts as a hydrogen evolution inhibitor, meaning it suppresses the formation of hydrogen gas during the electrochemical process. Before the HC process, a potentiodynamic scan has been performed for the two materials to determine the applied HC potential, as shown in Figure 1. Considering the specific

electrochemical properties of the sample's material, the potential range is from -1.3V to -0.6V. The potentiodynamic scan was performed at a rate of 1 mV per second. After these measurements, the corrosion potentials are known to be -816mV and -802mV, for 4420 and 4404 respectively. As for the charging potential, an overpotential of 150 mV above the corrosion potential has been chosen with the solution at 50 ° Celsius. The duration for HC is 72 hours.

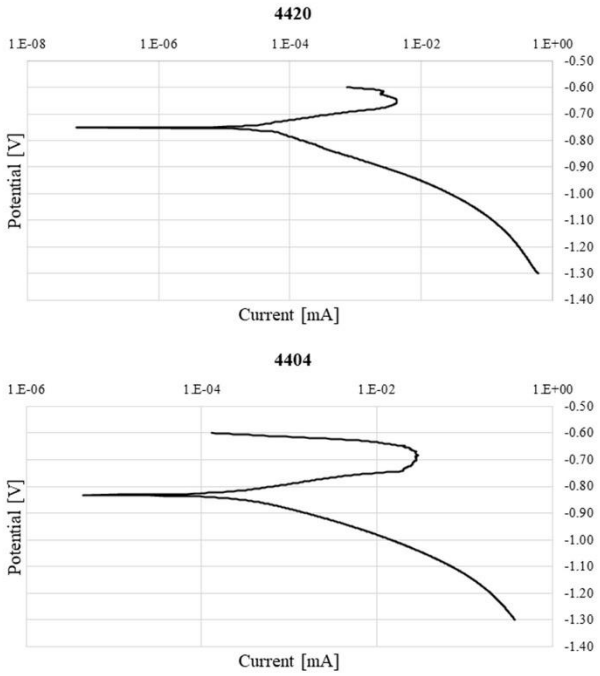

Figure 1 Potentiodynamic curves of 316L stainless steel 4420 and 4404.

2.3 Mechanical testing

The chosen constant crosshead velocity was 0.9 mm/min for tensile tests, and for the specimen gauge length of 30 mm, it corresponded to the quasi-static strain rate of $5 \times 10\text{-}3\ s^{-1}$ before necking. For the tensile tests, the SDB (Smooth Dog Bone) geometry was employed. The SDB geometry features a standard shape with a narrowed neck section and enlarged ends. The dimensions of the sample can be observed in Figure 2.

For the fracture tests, a strain rate of 0.45 mm/min was used. This design is to ensure similar quasi-static strain rates for the tensile tests and fracture tests, which have been carried out to evaluate the resistance of the material to crack propagation at different stress states. To cover a wide range of stress triaxialities, different specimen geometries are used in the test. Geometries such as NDB (Notched Dog Bone), CH (Centre Hole), and SH (Shear) have been used to address different loading modes and stresses in the tests. The choice of specific specimen geometries allows different stress states to be

simulated and provides a more complete understanding of the material's behavior in terms of toughness and fracture.

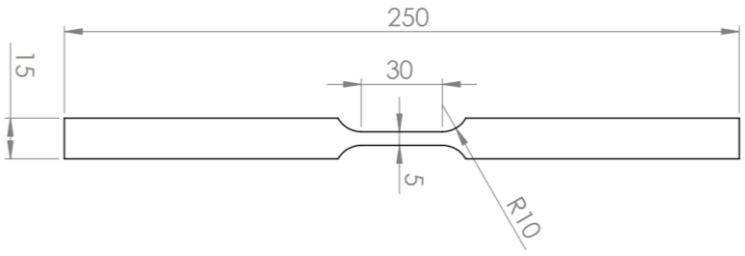

Figure 2 SDB geometry dimensions

To understand how this anisotropy affects the material, tensile tests have been carried out using SDB geometry in three different directions: 0 degrees, 45 degrees, and 90 degrees. In the 0˚ direction, the tensile force is applied parallel to the rolling direction (RD). This gives an assessment of the mechanical properties of the material in the main rolling direction. In the 90˚ direction, the tensile force is applied perpendicular to RD as the transverse direction (TD). The 45˚ direction is therefore the diagonal direction (DD).

NDB

The NDB geometries are used to evaluate fracture toughness under conditions of uniaxial stresses and stress concentration at the notch tip, as shown in Figure 3. The sample with a large notch radius (NDBR25) tends more towards uniaxial tension, while the one with a smaller notch radius (NDBR0.2) is closer to plane strain.

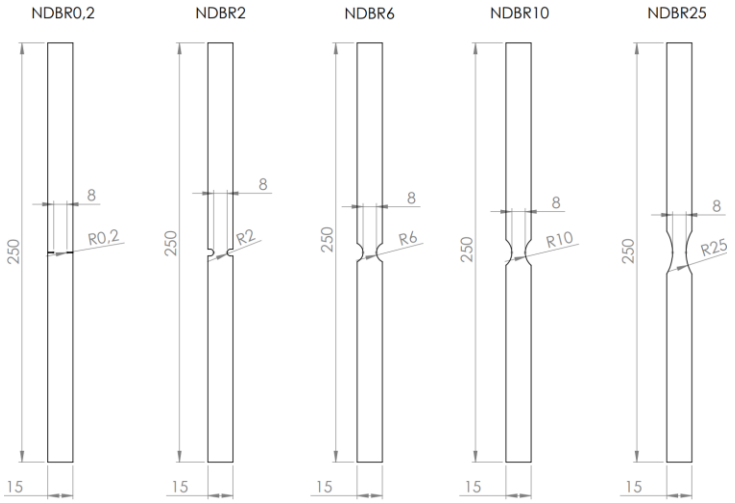

Figure 3 NDB geometries dimensions

CH

CH geometry is used to investigate the resistance to crack propagation in biaxial or radial stress situations, through the opening of a crack from the center of the specimen, as shown in Figure 4.

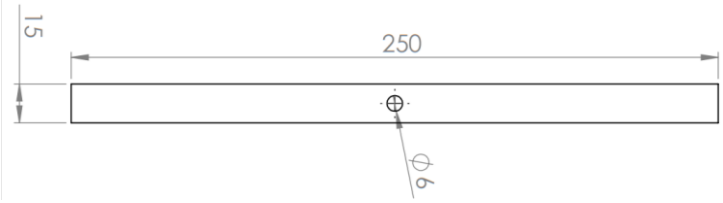

Figure 4 CH geometry dimensions

SH

Shear geometry is used to study creep resistance and crack propagation under pure shear loading conditions, as shown in Figure 5. This geometry involves the use of samples with a parallelogram cross-section or a specific shape that promotes the shearing of the material.

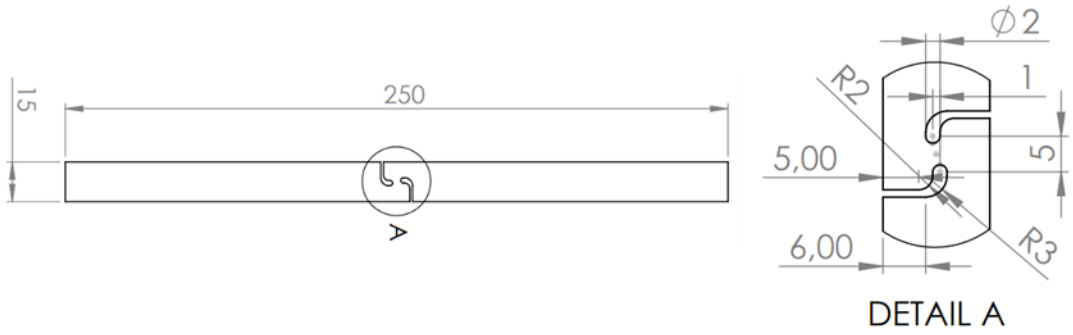

Figure 5 SH geometry dimensions

2.4 Microstructure characterization

To further reveal the underlying mechanism of two materials, electron backscatter diffraction (EBSD) was conducted for two original samples using JEOL JIB-4700F – NMC coupled with Oxford EBSD plug-in. Before the EBSD test, test samples were ground using 320#, 640#, and 1000# SiC sandpapers and then polished by an automotive polishing machine. The step size is set as 1 μm, and the scan area is 300 × 250 μm.

2.5 Thermal desorption spectroscopy (TDS)

A self-built TDS machine was applied in this study to measure the hydrogen absorption of 4420 and 4404 materials. All TDS measurements were performed at a heating rate of 10 °C/min. The total hydrogen concentration was calculated by integrating the area below the desorption rate versus the temperature curve.

3. Test result

3.1 Tensile test

Figure 6 shows the results of the anisotropy tests in the three directions (RD, TD, and DD) for 4420 and 4404. It can be observed that both 4404 and 4420 materials show anisotropy. It is also curious to mention that the RD in both cases is when the material presents the lowest ductility. This is possible because, during the cold rolling process, the grains of the material are aligned in the rolling direction. This means that the grains are preferentially oriented in the rolling direction and elongate in that direction. This alignment of the grains in the rolling direction can result in a higher mechanical strength in that direction due to a higher blocking of dislocations. However, it can also cause sliding of the crystalline planes to be more difficult and thus reduce the ductility in that direction. In contrast, in the transverse direction, the grains are not aligned in a preferential direction and their orientation is more random. This allows for greater movement of dislocations and easier sliding of the crystalline planes, which can lead to higher ductility in this direction. This difference in grain orientation and its impact on ductility is based on the crystalline structure of the material and the associated deformation mechanisms.

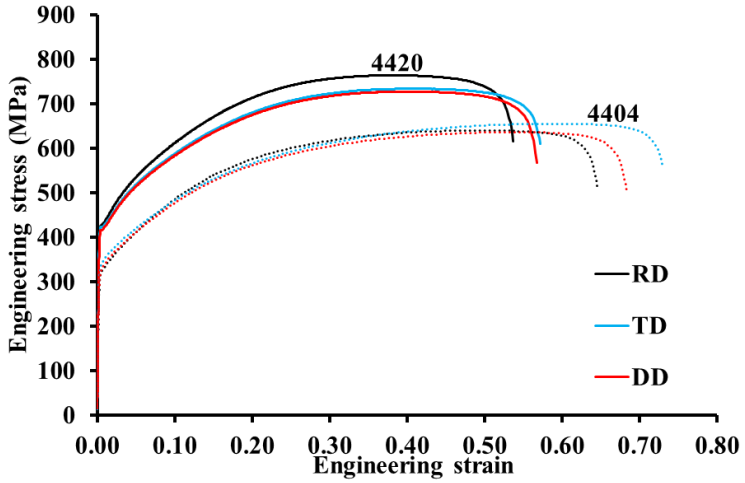

Figure 6 Engineering stress-strain curves of 316L stainless 4420 and 4404 steel with different directions.

Table 2 Data extracted from Figure 6

	4420-RD	4420-DD	4420-TD	4404-RD	4404-DD	4404-TD
Yield strength (MPa)	429.2	412.8	417.2	317.1	319.2	336.2

elongation (%)	54.0	56.9	57.2	65.1	68.6	73.2
Ultimate tensile strength (MPa)	763.3	712.6	733.9	639.7	636.1	655.1

Figure 7 and Table 3 show the results of the tensile tests for both materials, with and without HC. The test results clearly show that the presence of hydrogen has an impact mainly on the ductility of the material, while the rest of the stress values remain almost unchanged. This can be seen in the engineering stress-strain graphs, where a 4.33% ductility reduction in the plastic deformation capacity of the 4404 material and 1.79% for 4420 when exposed to hydrogen can be seen. The mechanical properties are summarised in the table below, and even in the samples with hydrogen, a minimally higher UTS is measured. Hydrogen atoms could interact with defects in the crystalline structure of the material and strengthen the bonds between metal atoms, increasing the resistance to deformation. All these results support the hypothesis that material 4420, with its modified chemical composition and higher corrosion resistance, has a higher resistance to hydrogen embrittlement compared to material 4404.

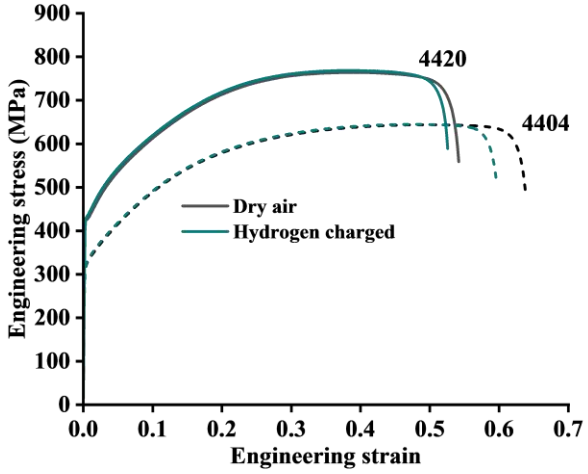

Figure 7 Engineering stress-strain curves of 316L stainless 4420 and 4404 steel in dry air condition and after hydrogen charged.

Table 3 Data extracted from Figure 7

	4420	4420-HC	4404	4404-HC

Yield strength (MPa)	429.2	429.8	317.1	317.3
elongation (%)	54.7	52.8	64.4	60
Ultimate tensile strength (MPa)	765	767	644	645

3.2 Fracture test

Figure 8 and Table 4 show the results of NDBR25 tests. As for 4404 specimens, a 6.2% loss in elongation capacity was observed after HC process. With respect to 4420, the displacement of samples go from 6.20 mm to 5.95 mm due to the effect of hydrogen, resulting in a loss of 4%.

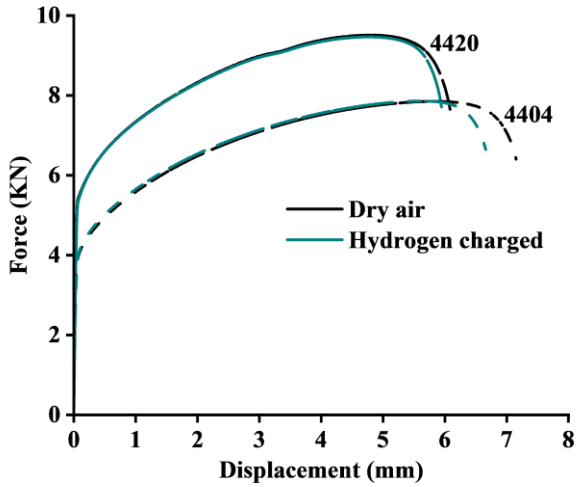

Figure 8 Displacement-Force curves for NDBR25

Table 4 Data extracted from Figure 8

	Condition	Displacement [mm]	Loss [%]
4420	Dry air	6.20	4.04
	Hydrogen charged	5.95	
4404	Dry air	7.22	6.17
	Hydrogen charged	6.77	

Figure 9 and Table 5 show the results of NDBR0.2 tests. Compared with NDBR25 sample, higher displacement loss is observed in NDBR0.2 samples for both 4420 and 4404 materials.

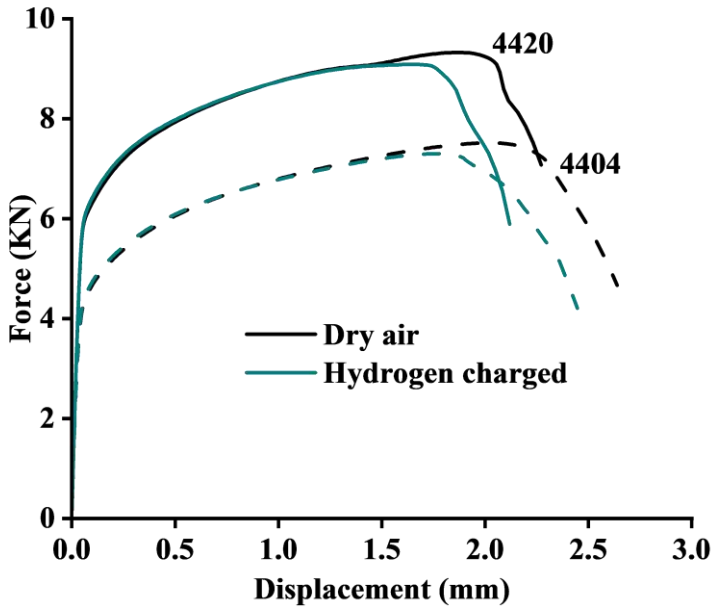

Figure 9 Displacement-Force curves for NDBR0.2

Table 5 Data extracted from Figure 9

	Condition	Displacement [mm]	Loss [%]
4420	Dry air	2.29	6.41
	Hydrogen charged	2.14	
4404	Dry air	2.75	10.98
	Hydrogen charged	2.44	

Figure 10 and Table 6 show the Displacement-Force curves for CHD6. The elongation loss of 4420 sample is slightly lower than that of 4404.

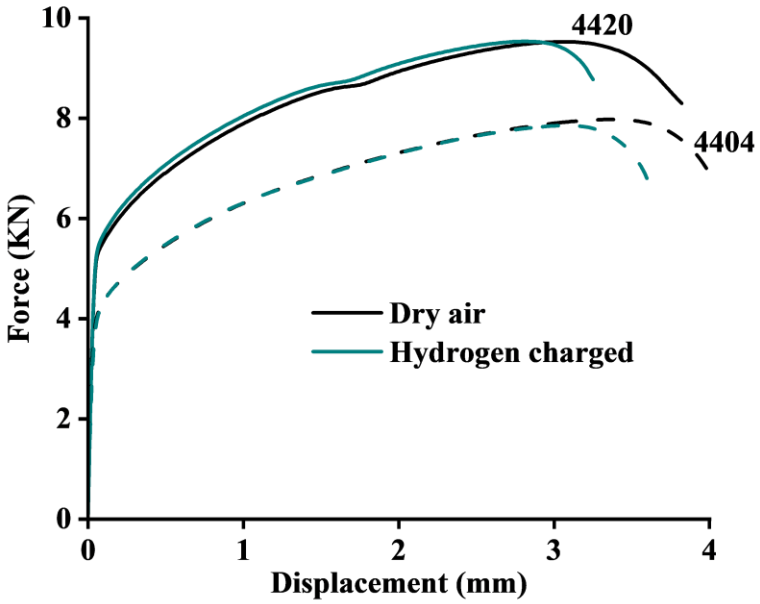

Figure 10 Displacement-Force curves for CHD6

Table 6 Data extracted from Figure 10 for CHD6

	Condition	Displacement [mm]	Loss [%]
4420	Dry air	3.82	9.42
	Hydrogen charged	3.46	
4404	Dry air	4.12	9.71
	Hydrogen charged	3.72	

Microstructure characterization

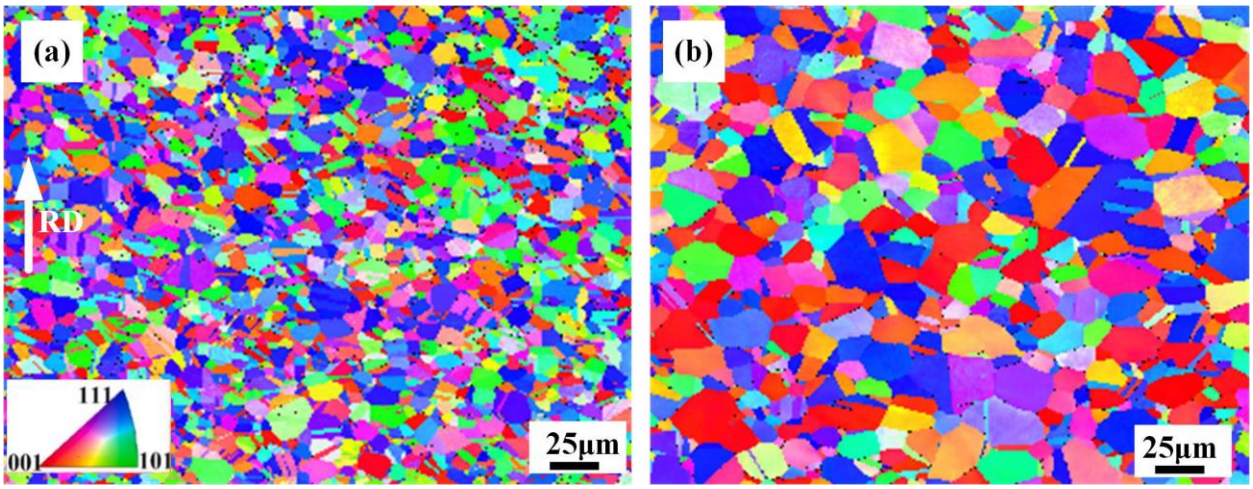

Figure 11 Inverse pole figure (IPF) of (a) 4420, (b) 4404

Figure 11 shows the IPF map of 4420 and 4404 materials. The average grain diameter of 4420 material is 2.19 and 8.43 μm, respectively. According to Hall-patch formula, the contribution of grain refinement (σ_G) could be calculated as:

$$\sigma_G = 181 + \frac{267}{\sqrt{D}} \quad (1)$$

Where D is the grain diameter. The value of σ_G is 361.8 MPa and 273.0 MPa for 4420 and 4404, respectively. Therefore, the higher yield strength of 4420 than 4404 can be ascribed to the finer grain size of 4420.

The higher hydrogen resistance of 4420 material could be explained by its lower grain size. However, further investigation is needed to make clear the underlying mechanism. Figure 12 shows the phase map of 4420 and 4404 materials. Small amounts of ferrite with bcc structure were detected in both 4420 and 4404 materials. The proportion of ferrite is 0.50% for 4420 material, and 0.38% for 4404, which plays a limited influence in the initial stage of the tensile test.

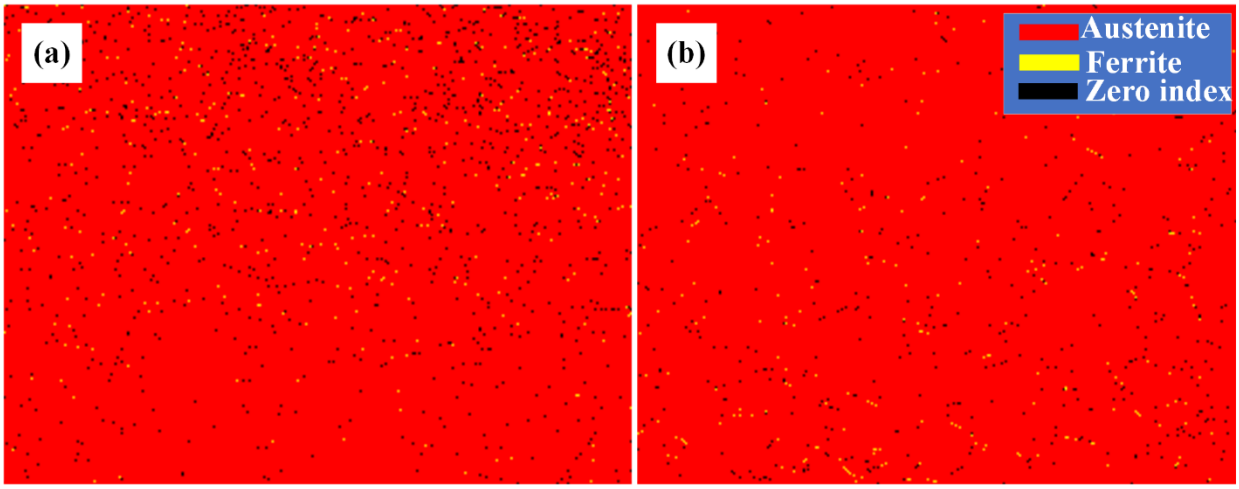

Figure 12 Phase map extracted from Figure 11: (a) 4420, (b) 4404.

Figure 13 shows the result after TDS test. The maximum hydrogen desorption rate of 4420 and 4404 is 5.09 and 3.69, respectively. It can be observed that the hydrogen absorption content of 4420 is higher than that of 4404, which can be attributed to the finer grain size and higher grain boundary density of 4420 material.

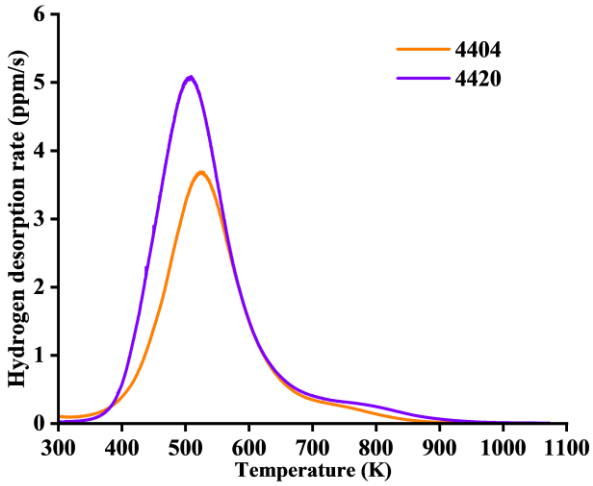

Figure 13 The relationship between temperature and hydrogen desorption rate.

Error! Reference source not found. shows the fracture surface of 4420 material with and without HC. Fine dimples are also observed in the fracture surface of 4420 material with and without HC, indicating that fracture model of 4420 material is ductile facture with and without HC process and the hydrogen diffusion did not change the fracture model of 4420 material in this research.

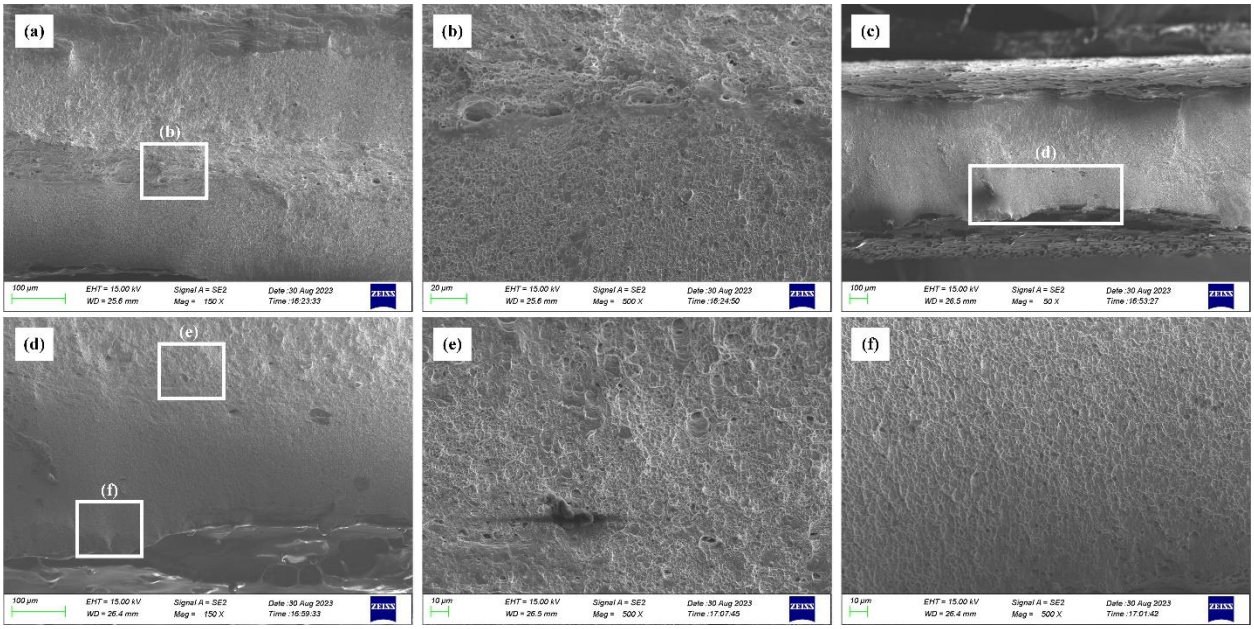

Figure 14 Fracture surface of (a) – (b) 4420 without HC, (c) – (f) 4420 with HC. The note near the white frame represents the corresponding enlargement images.

Figure 15 shows the fracuture surface of 4404 material without and with HC. As shown in Figure 15 (a) and (b), fine dimples are also observed in the fracture surface of 4404 material, indicating that fracture model of 4404 material is ductile facture. As shown in the Figure 15 (c) – (f), fine dimples are also observed in the 4404 material after hydrogen charging in the central area. However, flat facture surface is observed in the external area of 4404 material with HC, which indicate the hydrogen diffusion change the fracture model of the external area from ductile fracture to brittle fracture. This observation could explain the lower hydrogen resistance of 4404 material than that of 4420 material. However, what relieves the fracture model transformation process should be investigated in our next step research

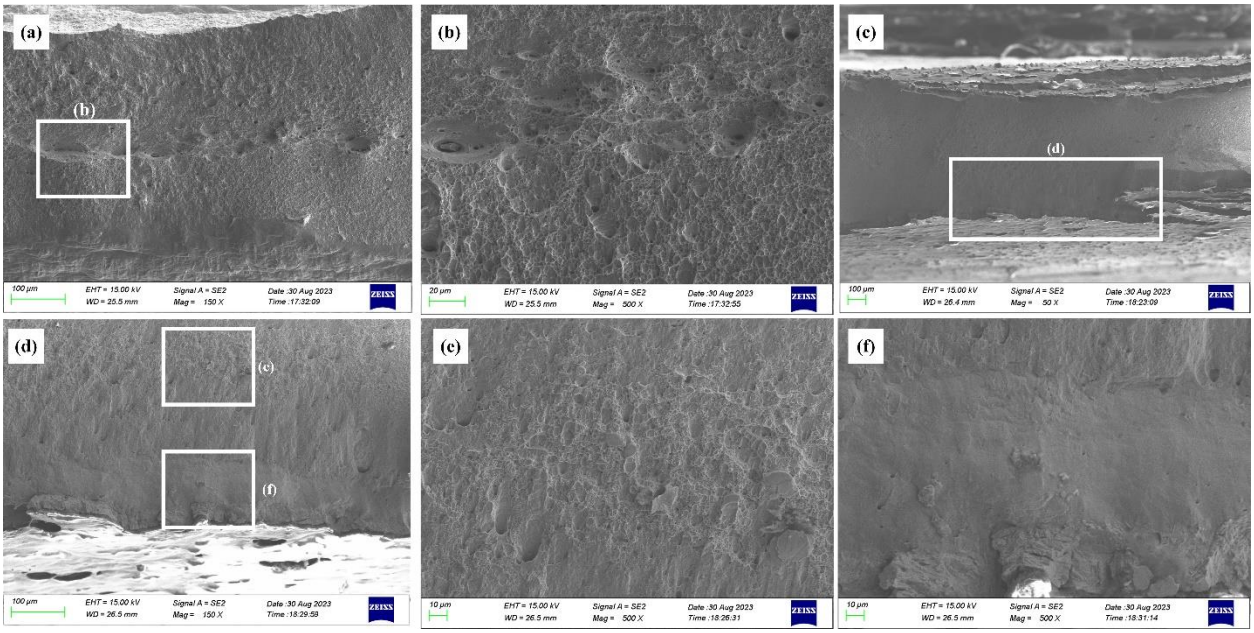

Figure 15 Fracture surface of (a) – (b) 4404 without HC, (c) – (f) 4404 with HC. The note near the white frame represents the corresponding enlargement images.

Conclusions

In summary, according to the displacement loss of tensile tests and fracture tests, the hydrogen embrittlement resistance of 4420 material is better than that of 4404 materials, which could be attributed to the brittle facture of 4404 material in the external area. Interestingly, the TDS result indicates the hydrogen absorption of 4420 is higher than that of 4404 in the HC process. This observation indicates that some factors relieve the effect of hydrogen atoms on the degration of mechanical properties of 4420 material. However, we currently only finish partial work, which is needed to be completed in the future.